Interhemispheric Differences in Polar Stratospheric HNO₃, H₂O, ClO, and O₃

M. L. Santee,* W. G. Read, J. W. Waters, L. Froidevaux,
G. L. Manney, D. A. Flower, R. F. Jarnot, R. S. Harwood,
G. E. Peckham

Simultaneous global measurements of nitric acid (HNO₃), water (H₂O), chlorine monoxide (ClO), and ozone (O₃) in the stratosphere have been obtained over complete annual cycles in both hemispheres by the Microwave Limb Sounder on the Upper Atmosphere Research Satellite. A sizeable decrease in gas-phase HNO₃ was evident in the lower stratospheric vortex over Antarctica by early June 1992, followed by a significant reduction in gas-phase H₂O after mid-July. By mid-August, near the time of peak ClO, abundances of gas-phase HNO₃ and H₂O were extremely low. The concentrations of HNO₃ and H₂O over Antarctica remained depressed into November, well after temperatures in the lower stratosphere had risen above the evaporation threshold for polar stratospheric clouds, implying that denitrification and dehydration had occurred. No large decreases in either gas-phase HNO₃ or H₂O were observed in the 1992–1993 Arctic winter vortex. Although ClO was enhanced over the Arctic as it was over the Antarctic, Arctic O₃ depletion was substantially smaller than that over Antarctica. A major factor currently limiting the formation of an Arctic ozone "hole" is the lack of denitrification in the northern polar vortex, but future cooling of the lower stratosphere could lead to more intense denitrification and consequently larger losses of Arctic ozone.

The severe depletion of stratospheric ozone over Antarctica (1) in late winter and early spring (the so-called Antarctic ozone "hole") is now known (2) to be caused by chlorine chemistry. Recently, there has been heightened concern about the possibility of a similar feature appearing in the Northern Hemisphere as the abundance of chlorine in the stratosphere continues to increase. Abundances of reactive chlorine, in the form of ClO, comparable to those over Antarctica (3) have been observed throughout the Arctic vortex (4), but the accompanying loss of O₃ over the Arctic has been much less severe (5) than that over Antarctica. The presence of HNO₃ affects the cumulative amount of chlorine-catalyzed O₃ destruction in two major ways. First, in the low temperatures of polar winter, HNO₃ condenses to form type I nitric acid trihydrate (NAT) polar stratospheric clouds (PSCs), which provide surfaces for the heterogeneous activation of chlorine. Second, photolysis of HNO₃ vapor releases nitrogen dioxide (NO₂), leading to chlorine deactivation through the formation of the reservoir species chlorine nitrate (ClONO₂). Type II water ice PSCs, which form if temperatures drop below the frost point, can also incorporate HNO₃ va-

por (6, 7). Removal of gas-phase HNO₃ from the lower stratosphere, either temporarily through condensation or permanently through the sedimentation of type I or type II PSC particles (denitrification), reduces the availability of NO₂ and allows chlorine to remain activated. Measurements of gas-phase HNO₃ have recently been obtained from the Microwave Limb Sounder (MLS) on the Upper Atmosphere Research Satellite (UARS) (8). Because MLS also provides data on ClO, O₃, and H₂O, we now have a global set of simultaneous, commonly calibrated measurements directly addressing the correlations between denitrification, dehydration, chlorine activation and deactivation, and ozone destruction.

The MLS instrument (9) acquires stratospheric measurements that are not degraded by PSCs or aerosols (10); MLS observations of ClO (4, 11), O₃ (4, 11–13), and H₂O (14) have been reported previously. Improved accuracy and an extended vertical range for the H₂O data reported here were achieved with a nonlinear, iterative retrieval scheme, yielding an estimated precision and absolute accuracy of ~0.2 parts per million by volume (ppmv) and ~15%, respectively, at 46 hPa (1 hPa = 100 Pa = 1 mbar), and of ~1.3 ppmv and ~100%, respectively, at 100 hPa. The measurement of HNO₃, a minor contributor in the 205-GHz spectral bands used to measure O₃ and ClO, was a secondary MLS objective (10). Vertical profiles of gas-phase HNO₃ are now being retrieved for the lower stratosphere and have improved the fits to the radiometric data (15). The MLS measure-

ments of HNO₃ have an estimated precision and absolute accuracy of ~2 parts per billion by volume (ppbv) and ~15%, respectively, at 46 hPa, and of ~2 ppbv and ~50%, respectively, at 100 hPa, and a vertical resolution of ~5 km. The Cryogenic Limb Array Etalon Spectrometer (CLAES) on UARS also measures HNO₃ (16). Initial comparisons of MLS and CLAES lower stratospheric HNO₃ show good agreement, generally to better than 30% at 46 hPa (15).

The evolution of MLS ClO, O₃, HNO₃, and H₂O in the Southern Hemisphere in 1992 is illustrated in Fig. 1. These particular days were selected to represent conditions before, during, and after the period in which stratospheric temperatures were low enough for PSCs. The MLS data are displayed on an isentropic [constant potential temperature (17)] surface to remove the effects of adiabatic vertical motions. We show the 465 K surface (~19 km) near the level of maximum O₃ depletion (12); surfaces at 520 K (~21 km) and 585 K (~24 km) have also been examined and exhibit similar behavior. Steep gradients in potential vorticity (PV) (18) on an isentropic surface demark the boundary of the polar vortex, so the proximity of the two PV contours in the maps indicates vortex strength. The southern polar vortex is already well established by 28 April. Relatively large concentrations of HNO₃, O₃, and H₂O are evident in the vortex interior at this time and can be attributed to the diabatic downward transport of air with higher mixing ratios of these species (19). Temperatures are still above the PSC formation threshold, and chlorine has not yet been activated.

Chlorine activation has begun by the time MLS looks south again (20) on 2 June as evidenced by the large ClO values in the sunlit portion of the vortex. Abundances of O₃ and H₂O inside the vortex have increased, consistent with continuing diabatic descent. Altitude changes in CLAES N₂O (21) mixing ratio contours between late April and mid-June confirm that descent is ongoing [N₂O is a dynamical tracer that develops horizontal gradients on isentropic surfaces in the presence of diabatic processes (22)]. Although diabatic descent is also expected to cause an increase in HNO₃ abundances, a deficit in gas-phase HNO₃ has developed, coincident with the region in which temperatures have fallen below the formation threshold (6) (~195 K) of NAT PSCs. Whether this deficit is indicative of the permanent removal of HNO₃ from the lower stratosphere (denitrification) or just the temporary sequestration of gas-phase HNO₃ in NAT PSCs cannot be ascertained from the MLS observations alone.

M. L. Santee, W. G. Read, J. W. Waters, L. Froidevaux, G. L. Manney, D. A. Flower, R. F. Jarnot, Mail Stop 183-701, Jet Propulsion Laboratory, California Institute of Technology, Pasadena, CA 91109, USA.
R. S. Harwood, Department of Meteorology, Edinburgh University, Edinburgh EH9 3JZ, UK.
G. E. Peckham, Department of Physics, Heriot-Watt University, Edinburgh EH14 4AS, UK.
*To whom correspondence should be addressed.

This is the earliest that HNO_3 condensation has been observed in southern winter. Because temperatures remain above the frost point at this time, a comparable decrease in H_2O vapor is not expected and indeed is not present in the MLS data. Although in situ observations of correlated low concentrations of water vapor and total reactive nitrogen over Antarctica (23) have been taken to imply that the processes of denitrification and dehydration are coupled, other observations (24) have been interpreted to suggest that denitrification can occur without significant dehydration. Theoretical studies (7, 25) have found that the sedimentation rate of HNO_3 particles can be sufficiently rapid—given low cooling rates or cooling to just below the NAT condensation point—for substantial HNO_3 loss to take place over short time scales, independent of the formation of water ice clouds. On the basis of temperature data collected during the 1987 southern winter, Salawitch et al. (25) calculate that extensive denitrification could have occurred by the first or second week in June, with significant dehydration occurring later. The MLS instrument does not detect HNO_3 or H_2O in condensed phase, but the significant decrease observed in gas-phase HNO_3 without a corresponding decrease observed in gas-phase H_2O is a necessary (albeit not sufficient) condition for the decoupling of these processes.

The MLS observations on 17 August (11) show ClO values of ~2 ppbv in most of the sunlit area poleward of 60°S and a ring of depleted O_3 coincident with the largest ClO abundances. Temperatures are below the formation threshold (6) of type II PSCs over most of the Antarctic continent, and gas-phase HNO_3 values are extremely low (≤ 2 ppbv) throughout this region. A "collar" of high HNO_3 (≥ 10 ppbv) is seen just outside the low-temperature region, consistent with previous aircraft observations (23, 26) and colocated CLAES measurements (16). The outer boundary of enhanced ClO roughly corresponds to the inner edge of the HNO_3 collar region, as expected from conversion of ClO into $ClONO_2$ through reaction with NO_2 supplied by HNO_3 photolysis. Depletion of H_2O vapor has been in progress since at least shortly before the end of the previous MLS south-looking period in mid-July (27); by mid-August, there is extensive loss of H_2O vapor within the low-temperature zone, where values range from about 1.5 to 3.5 ppmv, in good agreement with earlier aircraft observations inside the vortex in August and September (28). Again, the MLS data do not distinguish between the temporary formation of ice clouds and the permanent removal of HNO_3 or H_2O. However, NAT PSC particles can grow

large enough (7, 25) to experience rapid fallout, and the larger ice crystals of type II PSCs [which can also incorporate HNO_3 (6, 7)] sediment more readily. It is therefore likely that the Antarctic lower stratosphere has undergone both denitrification and dehydration by this time.

There are no MLS measurements over Antarctica from mid-September through the end of October (20). By the time south-viewing resumes on 1 November, chlorine over Antarctica has been largely deactivated. However, the O_3 deficit that developed in September (4, 11, 12) persists. The deficits in gas-phase HNO_3 and H_2O also persist, with mixing ratio values less than 6 ppbv and less than 3 ppmv, respectively, throughout most of the vortex. Similar H_2O values were measured by the UARS Halogen Occultation Experiment (HALOE) in mid-October 1992 (29). The strong PV gradient indicates that the vortex is still intact, inhibiting mixing between polar and midlatitude air. Lower stratospheric temperatures rose above the NAT PSC formation threshold the last week in September (30). The fact that gas-phase HNO_3 and H_2O values remain depressed long after the last PSCs would have been expected to evaporate strongly implies that irreversible re-
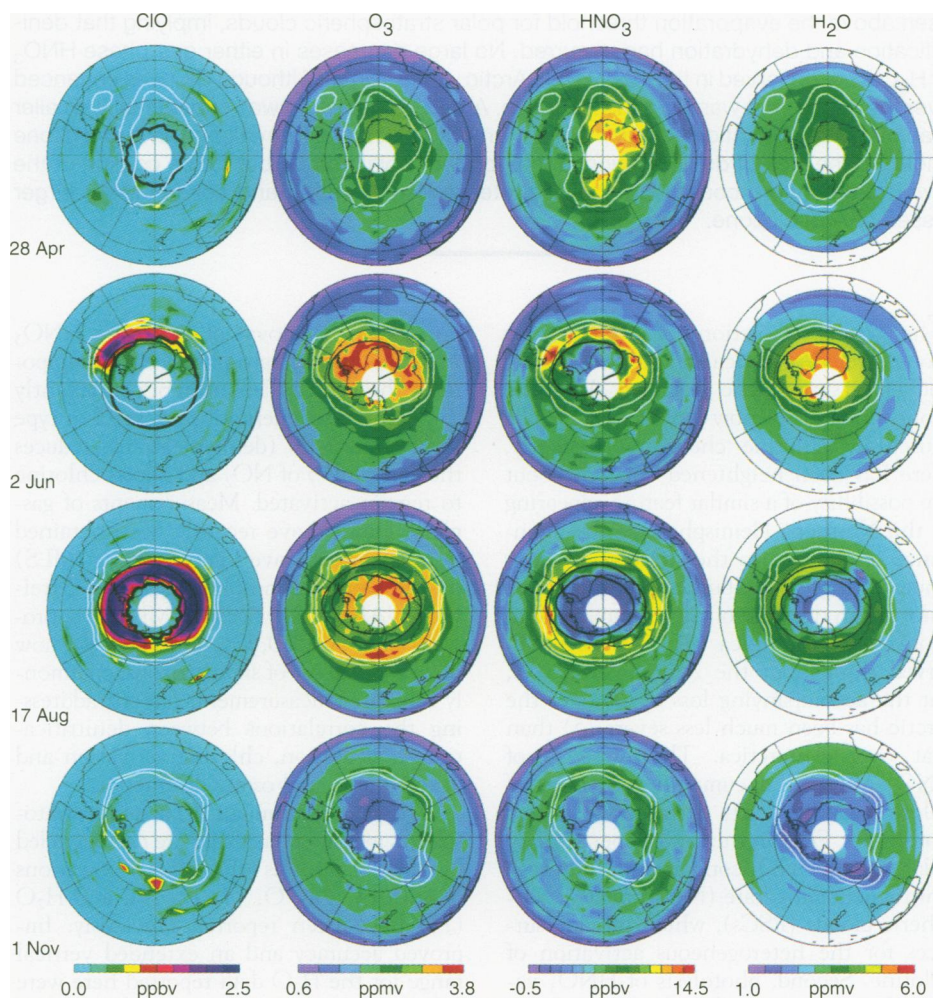

Fig. 1. Maps of MLS HNO_3, ClO, O_3, and H_2O for selected days during the 1992 southern winter, interpolated onto the 465 K potential temperature (17) surface with U.S. National Meteorological Center (NMC) temperatures. The maps are polar orthographic projections extending to the equator, with the Greenwich meridian at the top and black circles at 30° and 60°S. They were produced by linear interpolation of measurements taken over a 24-hour period. The nonlinear H_2O retrieval was performed poleward of 30°S, and no measurements were obtained in the white area poleward of 80°S. The thick black contours on the ClO maps identify the edge of daylight for the measurements; only data from the "day" side of the orbit are shown for ClO (34). Thin black lines show NMC temperature contours of 195 K (outer contour) and 188 K (inner contour), the approximate threshold temperatures (6) for type I and type II PSCs, respectively. Also superimposed (in white) on each of the maps are two contours of potential vorticity (PV) (18), calculated from NMC temperature and geopotential height fields. The outer contour (-2.5×10^{-5} K m^2 kg^{-1} s^{-1}) represents the approximate edge of the polar vortex during winter when it is well established (12); inclusion of the inner contour (-3.0×10^{-5} K m^2 kg^{-1} s^{-1}) provides information on the steepness of the PV gradient, indicating the strength of the vortex.

moval (denitrification and dehydration) occurred at this level.

This signature of denitrification and dehydration is not apparent in the 1992–1993 northern polar vortex (Fig. 2). In contrast to the Southern Hemisphere at the comparable season, on 26 October the northern vortex is not well established at 465 K. The PV gradient indicates that the vortex has increased substantially in size and strength by 3 December. Except for a small area over southern Finland, temperatures remain too high for PSCs, and ClO is not enhanced. Mixing ratios of O_3, HNO_3, and H_2O are relatively large inside the vortex at 465 K, again because of diabatic descent, and there is no evidence that condensation of HNO_3 has begun.

In late winter, there are striking differences between the hemispheres. Whereas the southern vortex in August is nearly centered over the pole, the northern vortex in February is distorted, with the southernmost portion covering most of Europe on 22 February. The ClO abundances are generally enhanced (>1 ppbv) throughout the vortex, but O_3 concentrations remain high,

suggesting that the replenishment by diabatic descent partly masks the destruction by chlorine chemistry (5). Between Greenland and Scandinavia, there is an area with temperatures below the NAT PSC threshold in which gas-phase HNO_3 abundances are low (about 5 to 9 ppbv) relative to the remainder of the vortex (about 10 to 14 ppbv). This low-temperature, low-HNO_3 region persists for only a few days. There is no corresponding perturbation in O_3 or ClO, implying that the sequestration of gas-phase HNO_3 in NAT PSCs, rather than intrusion of lower latitude air or uplift of the isentropes, causes the observed HNO_3 decrease. Compared to that for the Antarctic (Fig. 1), the Arctic reduction in gas-phase HNO_3 is less intense, more localized, and more transient, indicating that the Arctic vortex has not undergone significant denitrification. In addition, no significant decrease is observed in gas-phase H_2O.

Northern Hemisphere winters exhibit a high degree of interannual variability, and the 1992–1993 lower stratospheric vortex is characterized by below-average temperatures and anomalously strong PV gradients

(31). Therefore, the decrease in gas-phase HNO_3 in Fig. 2 is probably greater than that in most Arctic winters. By mid-March, after two strong stratospheric warmings (32), the high values of ClO have diminished. Ozone abundances are lower than in February, but the depletion is much less severe than that in the southern vortex between August and September (5). The continued presence of HNO_3 throughout the Arctic winter moderates the destruction of O_3 by providing a source of NO_2 to quench ClO.

Under present climate conditions, Arctic winter temperatures remain below the type I PSC threshold sufficiently long for lower stratospheric chlorine to be substantially converted to reactive form. However, they do not fall low enough or stay low long enough for sedimentation by either type I or type II PSC particles to cause extensive denitrification. Therefore, although ClO is enhanced over the Arctic as it is over Antarctica, the formation of an ozone "hole" over the Arctic has so far been limited by the lack of permanent removal of HNO_3. Future cooling of the lower stratosphere (for example, caused by increases in greenhouse gases) could intensify the loss of HNO_3 within the vortex and, while the chlorine loading remains high, lead to greater depletion of Arctic O_3 (33).

REFERENCES AND NOTES

1. J. C. Farman, B. G. Gardiner, J. D. Shanklin, Nature 315, 207 (1985); R. S. Stolarski et al., ibid. 322, 808 (1986).
2. M. B. McElroy and R. J. Salawitch, Science 243, 763 (1989); S. Solomon, Nature 347, 347 (1990); J. G. Anderson, D. W. Toohey, W. H. Brune, Science 251, 39 (1991).
3. R. L. de Zafra et al., Nature 328, 408 (1987); J. G. Anderson, W. H. Brune, M. H. Proffitt, J. Geophys. Res. 94, 11465 (1989).
4. J. W. Waters et al., Nature 362, 597 (1993).
5. G. L. Manney et al., ibid. 370, 429 (1994).
6. R. P. Turco, O. B. Toon, P. Hamill, J. Geophys. Res. 94, 16493 (1989).
7. O. B. Toon, R. P. Turco, P. Hamill, Geophys. Res. Lett. 17, 445 (1990).
8. C. A. Reber, ibid. 20, 1215 (1993); _____, C. E. Trevathan, R. J. McNeal, M. R. Luther, J. Geophys. Res. 98, 10643 (1993).
9. F. T. Barath et al., J. Geophys. Res. 98, 10751 (1993).
10. J. W. Waters, in Atmospheric Remote Sensing by Microwave Radiometry, M. A. Janssen, Ed. (Wiley, New York, 1993), chap. 8.
11. _____, L. Froidevaux, G. L. Manney, W. G. Read, L. S. Elson, Geophys. Res. Lett. 20, 1219 (1993).
12. G. L. Manney et al., ibid., p. 1279.
13. L. Froidevaux et al., J. Atmos. Sci. 51, 2846 (1994); L. S. Elson, G. L. Manney, L. Froidevaux, J. W. Waters, ibid., p. 2867.
14. R. S. Harwood et al., Geophys. Res. Lett. 20, 1235 (1993); W. A. Lahoz et al., J. Atmos. Sci. 51, 2914 (1994).
15. W. G. Read et al., unpublished results.
16. A. E. Roche, J. B. Kumer, J. L. Mergenthaler, Geophys. Res. Lett. 20, 1223 (1993); A. E. Roche et al., J. Atmos. Sci. 51, 2877 (1994).
17. Potential temperature (Θ), defined as the temperature an air parcel would have if it were expanded or compressed adiabatically to a pressure of 1000 hPa, is related to pressure p (in hPa) by $\Theta = T(1000/$
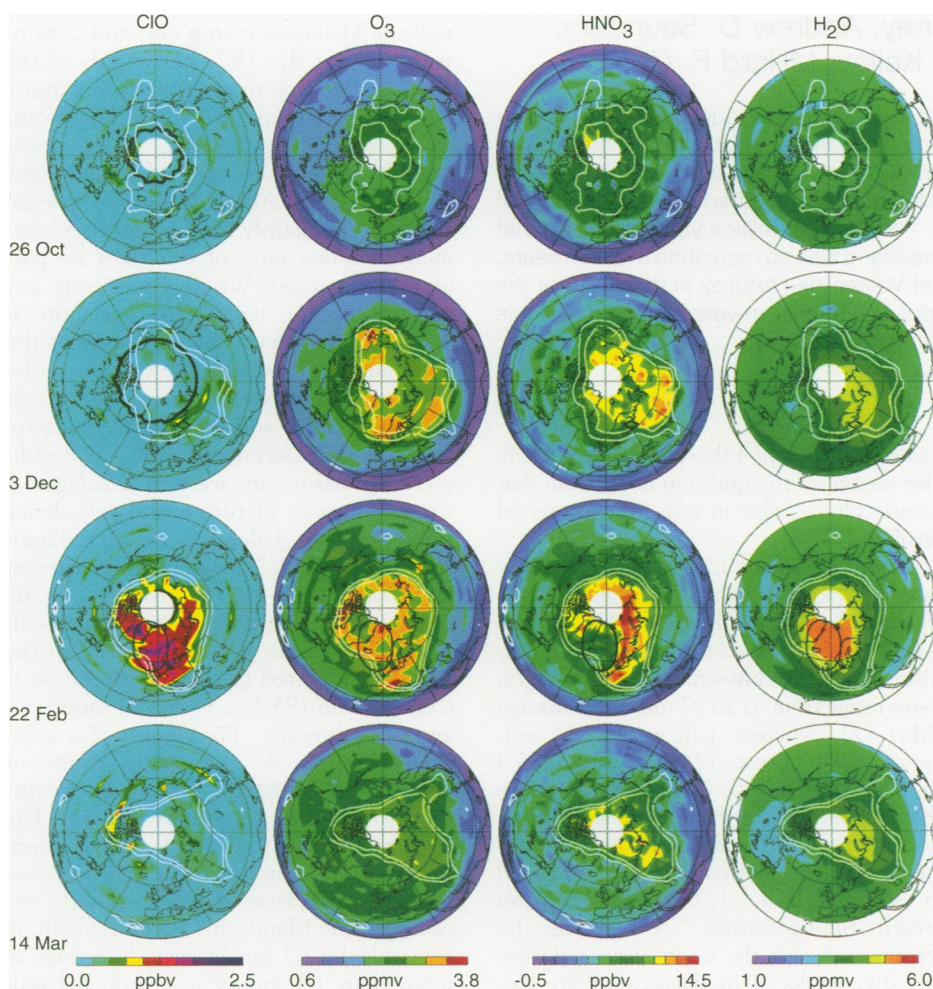
Fig. 2. As in Fig. 1, but for selected days during the 1992–1993 northern winter, with the Greenwich meridian at the bottom and positive PV contour values.

$p)^{0.286}$, where T is temperature in kelvin. Potential temperature is conserved under adiabatic conditions. For the low temperatures characteristic of the winter polar vortices, $\Theta = 465$ K corresponds to about $p = 50$ hPa and $\Theta = 585$ K corresponds to about $p = 22$ hPa.

18. Potential vorticity (PV) is defined as $PV = -g(f + \zeta) d\Theta/dp$, where g is the acceleration due to gravity, f is the Coriolis parameter, p is pressure, Θ is potential temperature (17), and ζ is the component of relative vorticity orthogonal to the Θ surface. For adiabatic, frictionless flow, PV is conserved, and contours of PV on potential temperature surfaces comprise the same air parcels.

19. M. R. Schoeberl and D. L. Hartmann, Science 251, 46 (1991).

20. The MLS pointing geometry and the inclination of the UARS orbit lead to measurement coverage from 80° on one side of the equator to 34° on the other. The UARS orbit plane precesses in such a way that all local solar times are sampled in about 36 days, after which the spacecraft is rotated 180° about its yaw axis. Thus, 10 times per year, MLS alternates between viewing northern and southern high latitudes.

21. J. B. Kumer, J. L. Mergenthaler, A. E. Roche, Geophys. Res. Lett. 20, 1239 (1993).

22. M. Loewenstein, J. R. Podolske, K. R. Chan, S. E. Strahan, J. Geophys. Res. 94, 11589 (1989); Geo-

23. D. W. Fahey et al., J. Geophys. Res. 94, 16665 (1989).

24. J. M. Rosen, S. J. Oltmans, W. F. Evans, Geophys. Res. Lett. 16, 791 (1989); P. Hamill and O. B. Toon ibid. 17, 441 (1990); G. Hübler et al., ibid., p. 453; S. R. Kawa, D. W. Fahey, L. C. Anderson, M. Loewenstein, K. R. Chan, ibid., p. 485; D. W. Fahey et al., Nature 344, 321 (1990); D. J. Hofmann and T. Deshler, J. Geophys. Res. 96, 2897 (1991).

25. R. J. Salawitch, G. P. Gobbi, S. C. Wofsy, M. B. McElroy, Nature 339, 525 (1989).

26. G. C. Toon et al., J. Geophys. Res. 94, 16571 (1989).

27. We cannot specify exactly when the decrease in H_2O commenced because the MLS 183-GHz radiometer used to measure H_2O was not operational for most of the second half of June and the first part of July 1992 because of a UARS solar array drive problem.

28. K. K. Kelly et al., J. Geophys. Res. 94, 11317 (1989); K. K. Kelly et al., Geophys. Res. Lett. 17, 465 (1990).

29. M. Bithell, L. J. Gray, J. E. Harries, J. M. Russell, A. Tuck, J. Atmos. Sci. 51, 2942 (1994).

30. Climate Analysis Center, National Meteorological Center, Southern Hemisphere Winter Summary, 1992, Selected Indicators of Stratospheric Climate (National Oceanic and Atmospheric Administration, Washington, DC, 1992).

31. G. L. Manney et al., Geophys. Res. Lett. 21, 2405 (1994).

32. G. L. Manney et al., ibid., p. 813.

33. W. H. Brune et al., Science 252, 1260 (1991); J. Austin, N. Butchart, K. P. Shine, Nature 360, 221 (1992).

34. The ClO abundances are much smaller on the "night" side of the orbit because of a lack of photolysis of the dimer Cl_2O_2, formed from ClO recombination.

35. We thank M. R. Schoeberl for encouraging us to pursue the MLS HNO_3 measurement; A. E. Roche and the CLAES team for N_2O data and for discussions and comparisons of HNO_3 data; National Meteorological Center (NMC) Climate Analysis Center personnel, especially M. E. Gelman and A. J. Miller, for making NMC data available to the UARS project; two anonymous referees for helpful comments; and our MLS colleagues, especially T. Lungu, R. P. Thurstans, and E. F. Fishbein. M.L.S. gratefully acknowledges a Resident Research Associateship from the National Research Council. The work at the Jet Propulsion Laboratory, California Institute of Technology, was sponsored by the National Aeronautics and Space Administration, and the work at Edinburgh University and Heriot-Watt University was sponsored by the Science and Engineering Research Council.

12 August 1994; accepted 22 November 1994

Timing of Hot Spot–Related Volcanism and the Breakup of Madagascar and India

Michael Storey,* John J. Mahoney, Andrew D. Saunders, Robert A. Duncan, Simon P. Kelley, Millard F. Coffin

Widespread basalts and rhyolites were erupted in Madagascar during the Late Cretaceous. These are considered to be related to the Marion hot spot and the breakup of Madagascar and Greater India. Seventeen argon-40/argon-39 age determinations reveal that volcanic rocks and dikes from the 1500-kilometer-long rifted eastern margin of Madagascar were emplaced rapidly (mean age = 87.6 ± 0.6 million years ago) and that the entire duration of Cretaceous volcanism on the island was no more than 6 million years. The evidence suggests that the thick lava pile at Volcan de l'Androy in the south of the island marks the focal point of the Marion hot spot at ~88 million years ago and that this mantle plume was instrumental in causing continental breakup.

Many of Earth's flood basalt provinces occur at the rifted margins of continents and can be linked to the initiation of oceanic hot spot tracks (1, 2). Flood basalt provinces have been interpreted as signaling the arrival of a new mantle plume (3) or, alternatively, as forming by extension over a preexisting shallow region of hot spot mantle (2), developed by the steady upwelling and accumulation of plume material beneath continental lithosphere (4). Debate also surrounds the question of the role that mantle plumes play in causing continental breakup (5).

The widespread Cretaceous flood basalts of Madagascar can be related to the track of the Marion hot spot (Fig. 1) (6); however, the precise timing of the volcanism is poorly known. Potassium-argon dates range from 31 to 97 million years ago (Ma) (7), whereas paleontological evidence (8, 9) suggests a Maastrichtian [65.4 to 71.3 Ma (10)] to Turonian age range (88.7 to 93.3 Ma) for the igneous activity. Possible correlative rocks are the numerous Cretaceous mafic dikes that are found in southwest India (11). In this report, we present high-precision $^{40}Ar/^{39}Ar$ age determinations for the Cretaceous volcanic and dike rocks of Madagascar. Plate-tectonic considerations favor an active, rather than a passive, role for the Marion

plume in the generation of this flood basalt province and the breakup of Madagascar and India.

The Cretaceous volcanic and intrusive rocks of Madagascar crop out semi-continuously along the 1500-km length of the east coast, which marks the rifted margin, and in the Majunga and Morondava basins in western Madagascar (Fig. 2). The rocks include basalt flows and dikes and some rhyolite flows. Along the rifted margin the flows lie mainly on Precambrian basement, whereas most of the dikes are parallel to the coast. Whether there are any seaward-dipping basalt flows offshore is unknown; however, the steepness of the rifted margin precludes the existence of a large volcanic wedge of the type that typifies most other volcanic passive margins, such as East Greenland (12). The sedimentary basins in western Madagascar record episodes of rifting and subsidence since the late Paleozoic (9, 13). Basalt flows crop out for 700 km in the northwest and 200 km in the southwest and are interbedded with Upper Cretaceous sedimentary rocks. In the Majunga Basin the flows are reported to occur between post-Cenomanian (93.3 to 98.5 Ma) sandstone and fossiliferous pre-Upper Turonian limestone (8). A dike swarm crops out adjacent to the basalt flows in the northern part of the Morondava Basin. The Volcan de l'Androy complex in southern Madagascar contains the thickest sequence of Cretaceous volcanic rocks exposed on the island; this massif is about 50 km wide by 90 km long and consists of more than 1.5 km of interbedded basalt and rhyolite, with microgranite outliers (14). To the west is the Ejeda-Bekily dike

M. Storey, Danish Lithosphere Center, Øster Voldgade 10, Copenhagen 1350, Denmark.
J. J. Mahoney, School of Ocean and Earth Science and Technology, University of Hawaii, 2525 Correa Road, Honolulu, HI 96822, USA.
A. D. Saunders, Department of Geology, University of Leicester, University Road, Leicester LE1 7RH, UK.
R. A. Duncan, College of Oceanography, Oregon State University, Corvallis, OR 97331, USA.
S. P. Kelley, Department of Earth Sciences, Open University, Walton Hall, Milton Keynes MK7 6AA, UK.
M. F. Coffin, Institute of Geophysics, University of Texas, Austin, TX 78759, USA.

*To whom correspondence should be addressed.